Prepared for submission to JCAP

Evolution of the spin parameter of accreting compact objects with non-Kerr quadrupole moment

Cosimo Bambi

Institute for the Physics and Mathematics of the Universe, The University of Tokyo, Kashiwa, Chiba 277-8583, Japan

E-mail: cosimo.bambi@ipmu.jp

Abstract. There is robust observational evidence supporting the existence of $5 - 20\ M_\odot$ compact bodies in X-ray binary systems and of $10^5 - 10^9\ M_\odot$ bodies at the center of many galaxies. All these objects are commonly interpreted as black holes, even is there is no direct evidence that they have an event horizon. A fundamental limit for a black hole in 4-dimensional general relativity is the Kerr bound $|a_*| \leq 1$, where a_* is the spin parameter. This is just the condition for the existence of the event horizon. The accretion process can spin a black hole up to $a_* \approx 0.998$ and some super-massive objects in galactic nuclei could be rapidly rotating black holes with spin parameter close to this limit. However, if these super-massive objects are not black holes, the Kerr bound does not hold and the accretion process can spin them up to $a_* > 1$. In this paper, I consider compact bodies with non-Kerr quadrupole moment. I study the evolution of the spin parameter due to accretion and I find its equilibrium value. Future experiments like the gravitational wave detector LISA will be able to test if the super-massive objects at the center of galaxies are the black holes predicted by general relativity. If they are not black holes, some of them may be super-spinning objects with $a_* > 1$.

Contents

1 Introduction

Today we have robust observational evidence for the existence of $5-20\ M_\odot$ compact objects in X-ray binary systems [1] and of $10^5-10^9\ M_\odot$ objects at the center of many galaxies [2]. The stellar-mass objects in X-ray binary systems are surely too heavy to be neutron or quark stars for any reasonable equation of state [3, 4]. At least some of the super-massive objects in galactic nuclei are too heavy and compact to be clusters of non-luminous bodies, since the cluster lifetime due to evaporation and physical collisions would be shorter than the age of the system [5]. All these objects are commonly interpreted as black holes (BHs), since they cannot be explained otherwise without introducing new physics. However, there is no direct observation evidence that they have an event horizon [6], while there are theoretical arguments suggesting that the final product of the gravitational collapse may be quite different from a classical BH [7–12].

In 4-dimensional general relativity, BHs are described by the Kerr solution and are completely specified by two parameters: the mass, M, and the spin angular momentum, J. Instead of J, one can use the specific spin angular momentum $a = J/M$, or the dimensionless spin parameter $a_* = J/M^2$. The fact that these objects have only two degrees of freedom is known as "no-hair" theorem [13–15] and implies that all the mass moments, $\mathcal{M}_l$, and all the current moments, $\mathcal{S}_l$, of the space-time can be written in term of M and J by the following simple formula [16, 17]:

$$\mathcal{M}_l + i\mathcal{S}_l = M\left(i\frac{J}{M}\right)^l . \tag{1.1}$$

As it was put forward by Ryan in [18, 19], by measuring the mass, the spin, and at least one more non-trivial moment of the gravitational field of a BH candidate, one over-constrains the theory and can test the Kerr BH hypothesis.

The possibility of testing the Kerr metric around astrophysical BH candidates with future experiments is quite extensively discussed in the recent literature. A constraint on the nature of these objects has been recently obtained by considering the mean radiative efficiency of AGN [20]. The detection of gravitational waves from the inspiral of a stellar-mass compact body into a super-massive object, the so-called extreme mass ratio inspiral (EMRI), can be used to put very interesting constraints [21–27]. Since the future gravitational wave detector LISA will be able to observe about $10^4 - 10^6$ gravitational wave cycles emitted by an EMRI while the stellar-mass body is in the strong field region of the super-massive object, the quadrupole moment of the latter will be measured with a precision at the level of $10^{-2} - 10^{-4}$ [23]. The metric around super-massive BH candidates can also be probed by observing their "shadow" [28–30]. Additional proposals to test the Kerr BH hypothesis involve the possible discovery of a stellar-mass BH candidate with a radio pulsar as companion [31], the study of the Kα iron lines [32], and the analysis of the X-ray spectrum of a geometrically thin and optically thick accretion disk [33].

A fundamental limit for a BH in general relativity is the Kerr bound $|a_*| \leq 1$. This is just the condition for the existence of the event horizon. The accretion process can spin a BH up to $a_* \approx 0.998$ [34] and many super-massive objects in galactic nuclei may be rapidly rotating BHs with spin parameter close to this limit [35–37]. Nevertheless, if these objects are not the BH predicted by general relativity, the Kerr bound does not hold. Interestingly, in this case the accretion process can easily spin them up to $a_* > 1$ [38]. Such a possibility is currently ignored in the literature. It is also neglected in those works in which it is not assumed that these objects are BHs and it is studied how future observations can test the Kerr metric. For experiments like LISA, that rely on matched filtering, this may be a serious problem.

In Ref. [39–42], I studied some features of the accretion process onto objects with $|a_*| > 1$. However, an important question to address is if objects with $|a_*| > 1$ can really form. In [38], I showed that deviations from the Kerr metric can have the accreting gas spin the body up to $a_* > 1$. I used the Manko–Novikov (MN) metric [43], which is a stationary, axisymmetric, and asymptotically flat exact solution of the vacuum Einstein's equation. It describes the exterior gravitational field of a rotating massive body with arbitrary mass multipole moments and has an infinite number of free parameters. However, it has the drawback that it is valid only for sub-extreme objects, with spin parameter $|a_*| < 1$. So, I showed that the equilibrium spin parameter a_*^{eq} must be larger than 1, but it was impossible to discuss the accretion process for $a_* > 1$, compute a_*^{eq}, and figure out the properties of the space-time when $a_* > 1$. An extension to include super-spinning objects, if it exists, is non-trivial. In the present paper, I overcome this problem by considering another metric, the Manko–Mielke–Sanabria-Gómez (MMS) solution [44, 45]. It is not as general as the MN metric, but it can be easily extended to discuss objects with $a_* > 1$.

The content of this paper is as follows. In Sec. 2, I present the MMS solution adapted to the case of super-spinning objects. In Sec. 3, I study the main properties of this space-time and I show that the evolution of the spin parameter for an object whose exterior gravitational field is described by the MMS metric can be calculated as in the case of a BH. In Sec. 4, I discuss the evolution of the spin parameter of an object with non-Kerr quadrupole moment, as a consequence of the accretion process. Sec. 5 is devoted to the discussion of the results presented in Sec. 4, while summary and conclusions are in Sec. 6. Throughout the paper I use units in which $G_N = c = 1$.

2 Exterior field of a rotating body with non-Kerr quadrupole moment

The Manko–Mielke–Sanabria-Gómez (MMS) metric [44, 45] is a stationary, axisymmetric, reflection-symmetric, and asymptotically flat exact solution of the Einstein–Maxwell equations. It includes, as special cases, the Kerr and the $\delta = 2$ Tomimatsu–Sato solutions. It is specified by five real parameters: the mass, M, the specific spin angular momentum, $a = J/M$, the electric charge, $\mathcal{Q}$, and two other parameters, b and μ. The latter of which determine the mass quadrupole moment, Q, and the magnetic dipole moment, $\mathcal{M}$. Since the MMS solution is reflection-symmetric, all the odd mass moments and the even current moments are identically zero. Here I am interested in the vacuum solution only, and I put $\mathcal{Q} = \mathcal{M} = 0$, which implies $\mu = 0$. The mass quadrupole moment of the gravitational field is

$$Q = Q_{\rm Kerr} - (d - \delta - ab)M\,, \tag{2.1}$$

where $Q_{\rm Kerr} = -a^2 M$ is the quadrupole moment of a BH and

$$\delta = -\frac{M^2 b^2}{M^2 - (a-b)^2}\,, \qquad d = \frac{M^2 - (a-b)^2}{4}\,. \tag{2.2}$$

In Refs. [44, 45], the metric is written in prolate spheroidal coordinates, which are suitable for slow-rotating objects. It can be adapted to fast-rotating objects by proceeding as for the $\delta = 2$ Tomimatsu–Sato metric [46]: one has to change the prolate spheroidal coordinates into oblate spheroidal coordinates. That can be achieved through the transformation:

$$x \to ix\,, \quad k \to -ik\,, \tag{2.3}$$

where i is the imaginary unit, i.e. $i^2 = -1$. The line element becomes

$$\begin{aligned} ds^2 \,=\, & -f\,(dt - \omega d\phi)^2 + \frac{k^2 e^{2\gamma}}{f}\,(x^2 + y^2)\left(\frac{dx^2}{x^2+1} + \frac{dy^2}{1-y^2}\right) + \\ & + \frac{k^2}{f}\,(x^2+1)\,(1-y^2)\,d\phi^2\,, \end{aligned} \tag{2.4}$$

where $k = \sqrt{-d - \delta}$ and

$$f = \frac{A}{B}\,, \quad \omega = -(1-y^2)\frac{C}{A}\,, \quad e^{2\gamma} = \frac{A}{16k^8(x^2+y^2)^4}\,. \tag{2.5}$$

The functions A, B, and C can be written in the following compact way [45]

$$A = R^2 + \lambda_1\lambda_2 S^2\,, \quad B = A + RP + \lambda_2 ST\,, \quad C = RT - \lambda_1 SP\,. \tag{2.6}$$

Here $\lambda_1 = k^2(x^2+1)$, $\lambda_2 = y^2 - 1$, and

$$\begin{aligned} P \,=\, & 2kMx[(2kx+M)^2 - 2y^2(2\delta + ab - b^2) - a^2 + b^2] - 4y^2(4\delta d - M^2 b^2)\,, \\ R \,=\, & 4[k^2(x^2+1) + \delta(1-y^2)]^2 + (a-b)[(a-b)(d-\delta) - M^2 b](1-y^2)^2\,, \\ S \,=\, & -4\{(a-b)[k^2(x^2+y^2) + 2\delta y^2] + y^2 M^2 b\}\,, \\ T \,=\, & 8Mb(kx+M)[k^2(x^2+1) + \delta(1-y^2)] + \\ & + (1-y^2)\{(a-b)(M^2b^2 - 4\delta d) - 2M(2kx+M)[(a-b)(d-\delta) - M^2 b]\}\,. \end{aligned} \tag{2.7}$$

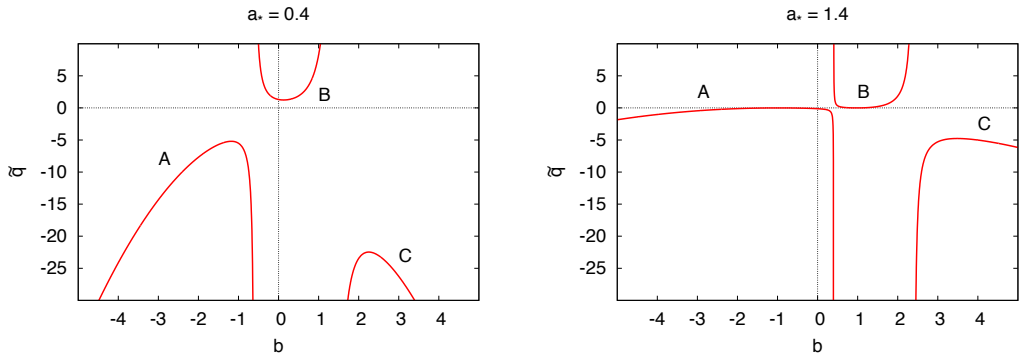

Figure 1. $\tilde{q} = (d - \delta - ab)/a^2$ as a function of the parameter b for $a_* = 0.4$ (left panel) and $a_* = 1.4$ (right panel). The Kerr solution is recovered for $b = \pm\sqrt{a^2 - M^2}$. b is given in units of $M = 1$.

In general, the mass quadrupole moment of an object depends on its mass and on its spin angular momentum in a non-trivial way, according to the specific properties of the matter the body is made of. In this paper, I will use the following definition of anomalous quadrupole moment $\tilde{q}$

$$Q = -(1 + \tilde{q})a^2 M \,. \tag{2.8}$$

For $\tilde{q} = 0$, one finds $Q = Q_{\rm Kerr}$, while for $\tilde{q} > 0$ ($\tilde{q} < 0$) the object is more oblate (prolate) than a BH. Eq. (2.8) is what we expect for neutron stars, with $\tilde{q} \approx 1 - 10$, depending on the equation of state and the mass of the body [47]. It is reasonable to assume that $\tilde{q} \geq -1$, since otherwise the effect of the rotation would make the body more and more prolate. For given M and a, the MMS solution does not allow for any arbitrary value of the anomalous quadrupole moment. In Fig. 1, I show $\tilde{q} = (d - \delta - ab)/a^2$ as a function of b for $a_* = 0.4$ (left panel) and $a_* = 1.4$ (right panel). There are three distinct curves: one in the region $b < a - M$ (curve A), one in the region $a - M < b < a + M$ (curve B), and the last one for $b > a + M$ (curve C). The equation $\tilde{q} = (d - \delta - ab)/a^2$ may have no real solutions for b (when $|a_*| < 1$), and up to four distinct real solutions (for $\tilde{q}$ sufficiently small). The Kerr metric is recovered for $b^2 = a^2 - M^2$. Two or more distinct solutions with the same M, a, and $\tilde{q}$ correspond to objects with the same mass, spin, and quadrupole moment, but with different higher order moments. A particular solution requires prolate spheroidal coordinates if $d + \delta > 0$ and oblate spheroidal coordinates if $d + \delta < 0$; otherwise, the constant k becomes an imaginary number. Generally speaking, slow-rotating solutions require prolate spheroidal coordinates, while fast-rotating solutions need oblate spheroidal coordinates; however, the critical value a_*^{crit} separating the two cases depends on $\tilde{q}$ and can be either larger or smaller than 1. In the rest of the paper, I will study the evolution of the spin parameter of objects with $\tilde{q} \geq -1$ and therefore I will discuss the solutions of b belonging to the curve A and B. When I find two solution with the same quadrupole moment, I will call the solution with smaller $|b|$, MMS1, and the other, MMS2.

3 Properties of the MMS solution

3.1 Structure of the space-time

The structure of the MMS space-time reminds one of the Tomimatsu–Sato and MN solutions [24, 48]. One finds naked singularities and closed time-like curves very close to the

massive object. The idea is that all these pathological features do not exist because inside the compact object, where the MMS metric, which is a vacuum solution, does not hold. Moreover, for $|a_*| < a_*^{eq}$ these pathological regions are always inside the inner radius of the disk and therefore they do not play any role in the discussion of the accretion process.

The infinite redshift surface $g_{tt} = 0$ determines the boundary of the ergoregion, which is not a pathological region and exists even around a rotating BH. Figs. 2, 3, and 4 show the ergosphere (red solid curve) for some MMS solutions with different value of the spin parameter and of the anomalous quadrupole moment. I use quasi-cylindrical coordinates ρz, see App. A. The topology of the ergoregion can change significantly as a_* and $\tilde{q}$ vary. The same figures show also the boundary of the closed time-like curve regions (blue dotted curves), defined by $g_{\phi\phi} = 0$. For small deviations from the Kerr metric (Fig. 2, $\tilde{q} = 0.01$), the shape of the ergoregion is very similar to the Kerr case, see App. B, but there are one or two small holes, where $g_{tt} < 0$. Every hole of the ergoregion can be associated with a small region with closed time-like curves, even if the boundaries of the holes and of the closed time-like curve regions do not coincide. For $\tilde{q} = 1.0$ (Fig. 3), there are two disconnected ergoregions[1] with no holes and one closed time-like curve region. For $\tilde{q} = -1.0$ (Fig. 4), one finds two ergoregions and one closed time-like curve region for the MMS1 solutions (left panels) and one ergoregion with a hole and two distinct closed time-like curve regions for the MMS2 solutions (right panels). Let us notice that the MMS1 solutions with $(a_*, \tilde{q}) = \{(0.98, 0.01), (0.8, 1.0), (1.2, 1.0)\}$ require prolate spheroidal coordinates, while all the other cases need oblate spheroidal coordinates. As the spin parameter increases, ergoregions and closed time-like curve regions move to larger ρ, but this is just an artifact of the coordinate system, see App. A.

3.2 Geodesic motion

The MMS space-time is stationary and axisymmetric. There are thus two constants of motion associated respectively with the t- and ϕ-coordinate; that is, the specific energy E and the specific axial component of the angular momentum L:

$$E = -g_{tt}\dot{t} - g_{t\phi}\dot{\phi}\,, \quad L = g_{t\phi}\dot{t} + g_{\phi\phi}\dot{\phi}\,, \tag{3.1}$$

where the dot denotes the derivative with respect an affine parameter. From (3.1), we have

$$\dot{t} = \frac{E g_{\phi\phi} + L g_{t\phi}}{g_{t\phi}^2 - g_{tt} g_{\phi\phi}}\,, \quad \dot{\phi} = -\frac{E g_{t\phi} + L g_{tt}}{g_{t\phi}^2 - g_{tt} g_{\phi\phi}}\,. \tag{3.2}$$

By substituting $\dot{t}$ and $\dot{\phi}$ into the equation of the conservation of the rest mass, $g_{\mu\nu}\dot{x}^\mu\dot{x}^\nu = -1$, we find

$$\frac{e^{2\gamma}}{f}\left(\frac{\dot{x}^2}{x^2+1} + \frac{\dot{y}^2}{1-y^2}\right) = \frac{e^{2\gamma}}{f}(\dot{\rho}^2 + \dot{z}^2) = V_{\rm eff}(\rho, z, E, L) \tag{3.3}$$

where

$$V_{\rm eff} = \frac{E^2}{f} - \frac{f}{\rho^2}(L - \omega E)^2 - 1\,. \tag{3.4}$$

[1] The fact that there are two disconnected ergoregions may depend on the coordinate system, as in prolate spheroidal coordinates the Schwarzschild radius $r = M$ reduces to the segment $|\rho| < \sqrt{a^2 - M^2}$ and $z = 0$ and the region with $r < M$ is not included, see App. A. The existence of these ergoregions should also be taken with caution, because close to the pathological region with closed time-like curves.

Since the left-hand side of Eq. (3.3) is non-negative, the motion of a test-particle is restricted to the region $V_{\rm eff} \geq 0$. The zeros of the effective potential $V_{\rm eff}$ are shown in Figs. 5 and 6 (orange dashed-dotted curves) for $a_* = 1.2$, $\tilde{q} = 1.0$ (MMS1), and different values of E and L. They indicate the boundary of the allowed regions of the motion. The blue dotted curves denote the boundaries of the closed time-like curve regions and must be inside the object. In Fig. 5, top panels, oblate spheroidal coordinates xy are used. The bottom panels are enlargements of the region close to the compact object in quasi-cylindrical coordinates ρz.

For $E = 1$ and large L (right panels in Fig. 5), we find an unbound region extending to infinity and a plunging region close to the massive object. As L decreases, the unbound region moves closer to the plunging region and a new allowed region of motion appears (central panels of Fig. 5). The latter has no counterpart in the Kerr space-time, while it exists in the MN case [24]. For smaller L (left panels of Fig. 5), the unbound region merges with the plunging one.

For $E < 1$, the situation is similar. In general, one find a bound region and a plunging region (central panel of Fig. 6). As L decreases, the bound region approaches the plunging region and eventually merges with the latter (left panel of Fig. 6). On the other hand, for larger values of L there is the plunging region only (right panel of Fig. 6).

In conclusion, the behavior of the geodesic motion is not very different from the Kerr and MN space-times. In particular, one can expect that the standard picture of the accretion process is correct: the particles of the gas approach the compact objects by losing energy and angular momentum. When they are at the innermost stable circular orbit (ISCO), they quickly plunge to the object[2].

In addition to E, L, and the rest mass, in the Kerr space-time there is a fourth constant of motion, the Carter constant $\mathcal{C}$ [49]. Its existence allows for the full separability of the equations of motion and it is a major source of research in modern day EMRI modeling. For a generic space-time, the existence of an effective fourth constant of motion can be checked by studying the Poincaré maps for geodesic motion of bound orbits: if they are all closed curves, there is a fourth constant of motion [24]. In analogy with the case of the MN solution discussed in [24], presumably even in the MMS space-time all orbits are strictly speaking chaotic, and no true fourth integral exists, but most of the orbits appear to be regular and one can find a quantity that is nearly invariant along them.

4 Evolution of the spin parameter

In this section, I compute the evolution of the spin parameter of the compact object due to the accretion process from a thin disk following Ref. [50]. I assume that the disk is on the equatorial plane of the object[3] and that the disk's gas moves on nearly geodesic circular orbits. The gas falls to the central object by loosing energy and angular momentum.

[2]This picture is surely correct for $\tilde{q} \geq 0$, as the radius of the ISCO is always determined by the orbital stability along the radial direction. For $\tilde{q} < 0$, the radius of the ISCO may depend on the stability of the orbit along the vertical direction, see e.g. the discussion in Refs. [33, 38]. In this second case, the gas particles reach the ISCO and then leave the equatorial plane. They plunge to the compact object after having lost additional energy and angular momentum. Such an additional loss of energy and angular momentum seems to be negligible in the description of the accretion process, but that should be checked in future studies by performing hydrodynamical and magnetohydrodynamical simulations.

[3]This assumption is correct for long term accretion onto a super-massive object at the center of a galaxy, since the alignment timescale of the spin of the object with the disk is typically much shorter than the accretion timescale [38].

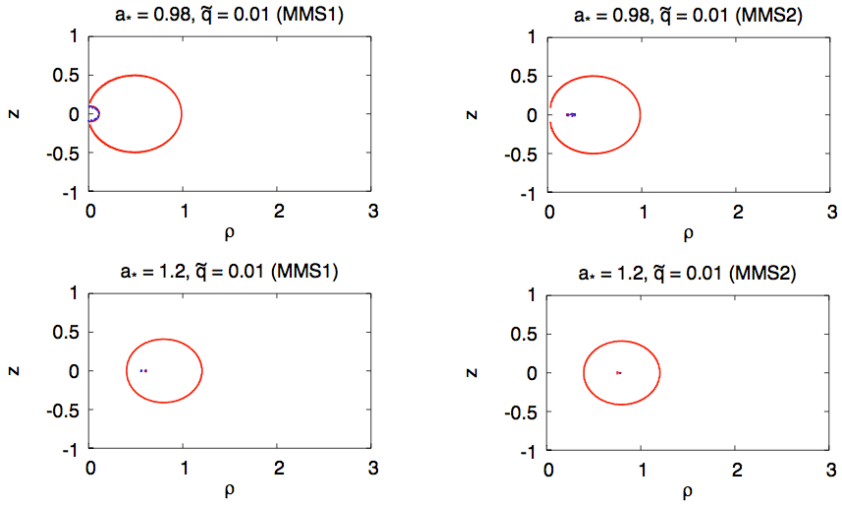

Figure 2. Space-time structure of the MMS solution for $\tilde{q} = 0.01$ and spin parameter $a_* = 0.98$ (top panels) and $a_* = 1.2$ (bottom panels). The solid red curves denote the infinite redshift surface $g_{tt} = 0$, defining the boundary of the ergoregion of the space-time. The dotted blue curves define the boundary of the causality violating region, where $g_{\phi\phi} < 0$. ρ and z are given in units of $M = 1$.

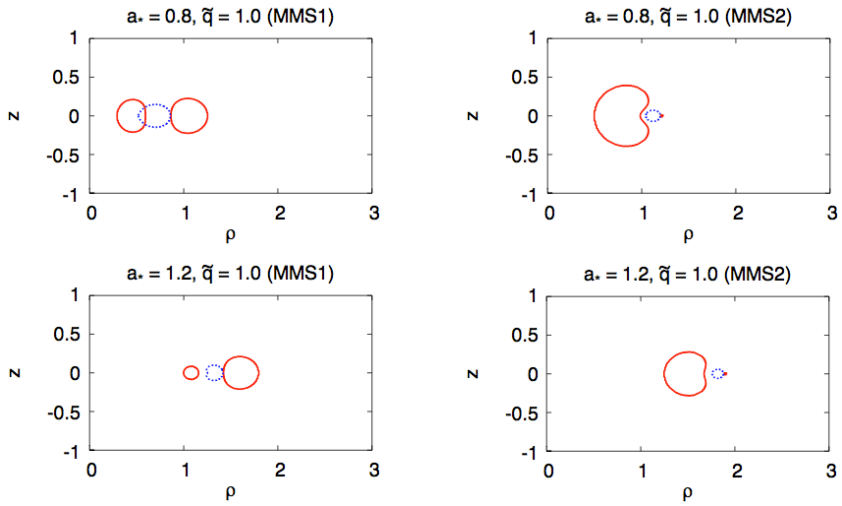

Figure 3. As in Fig. 2, for $\tilde{q} = 1.0$ and spin parameter $a_* = 0.8$ (top panels) and $a_* = 1.2$ (bottom panels).

When it reaches the ISCO, it plunges to the massive body. If the gas is "absorbed" by the compact object, with no further emission of radiation, the compact object changes its mass by $\delta M = E_{\rm ISCO}\delta m$ and its spin angular momentum by $\delta J = L_{\rm ISCO}\delta m$, where $E_{\rm ISCO}$ and $L_{\rm ISCO}$ are respectively the specific energy and the specific angular momentum of the gas particle at the ISCO, while δm is the gas rest-mass. The evolution of the spin parameter turns out to be governed by the following equation [50]

$$\frac{da_*}{d\ln M} = \frac{1}{M}\frac{L_{\rm ISCO}}{E_{\rm ISCO}} - 2a_* \,. \tag{4.1}$$

In the case of a body with a solid surface made of ordinary matter (i.e. protons, neutrons,

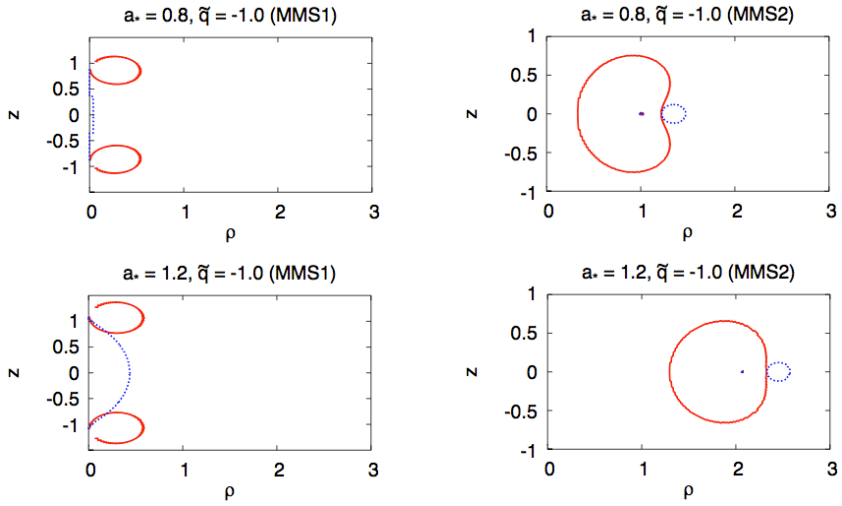

Figure 4. As in Fig. 3, for $\tilde{q} = -1.0$.

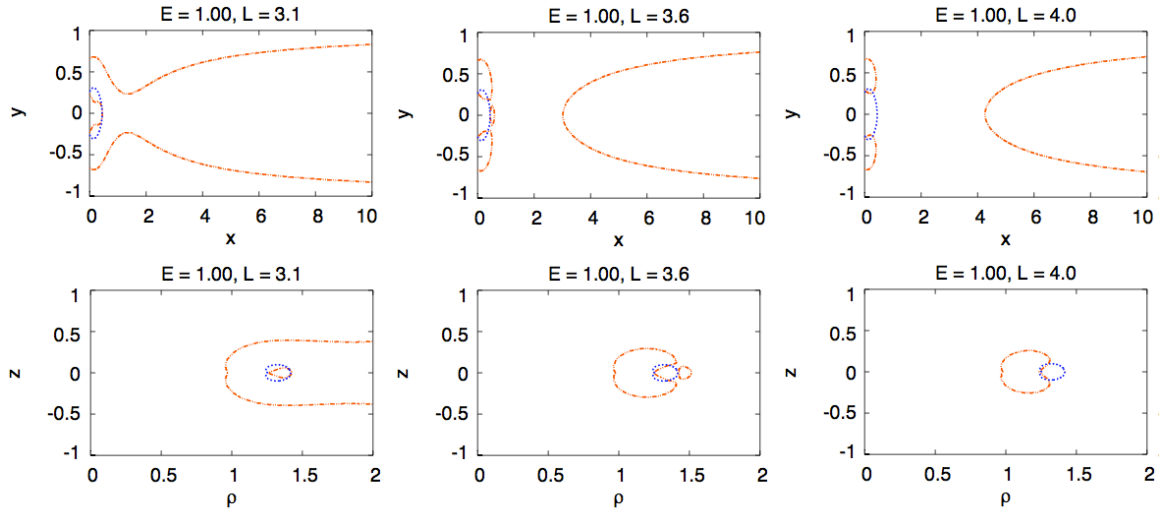

Figure 5. Effective potential for geodesic motion around a super-spinning object with $a_* = 1.2$ and $\tilde{q} = 1.0$ (solution MMS1) for $E = 1.00$ and $L = 3.1$ (left panels), $L = 3.6$ (central panels), and $L = 4.0$ (right panels). Top panels: xy-plane. Bottom panels: enlargement of the region closer to the object on the ρz-plane. The dashed-dotted orange curves denote the zeros of the effective potential; dotted blue curves indicate the boundary of the causality violating region, where $g_{\phi\phi} < 0$. L, ρ, and z are given in units of $M = 1$.

and electrons), this picture is not rigorously correct: the gas particles hit the surface of the body and release their gravitational energy in form of radiation. They are also accumulated on the surface and may undergo nuclear reactions, with the production of bursts. In such a situation, the computation of the evolution of the spin parameter is much more complicated and model dependent. On the contrary, if the compact object is a BH, the gas particles are really absorbed without further emission of radiation, since the BH has no solid surface, and, once the particles are behind the event horizon, their radiation cannot escape to infinity. For

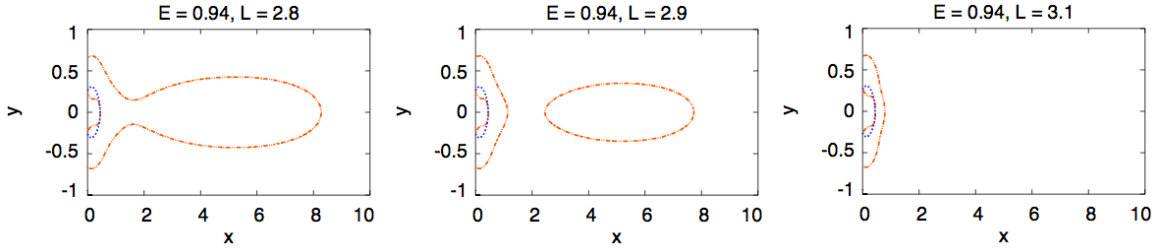

Figure 6. As in Fig. 5, for $E = 0.94$ and $L = 2.8$ (left panel), $L = 2.9$ (central panel), and $L = 3.1$ (right panel) on the xy-plane.

a BH, one can analytically integrate Eq. (4.1) and obtain [50]

$$a_* = \sqrt{\frac{2}{3}}\frac{M_0}{M}\left[4 - \sqrt{18\frac{M_0^2}{M^2} - 2}\right] \quad \text{for } M \leq \sqrt{6}M_0\,,$$
$$a_* = 1 \quad \text{for } M > \sqrt{6}M_0\,, \tag{4.2}$$

assuming an initially non-rotating BH with mass M_0. The equilibrium is reached for $a_*^{eq} = 1$ after the BH has increased its mass by a factor $\sqrt{6} \approx 2.4$. Including the effect of the radiation emitted by the disk and captured by the BH, one finds $a_*^{eq} \approx 0.998$ [34], because radiation with angular momentum opposite to the BH spin has larger capture cross section. The presence of magnetic fields in the plunging region may further reduce this value to $a_*^{eq} \sim 0.95$ [51, 52], by transporting angular momentum outward.

For astrophysical BH candidates, we can presumably use Eq. (4.1). They indeed seems to be capable of absorbing the accreting gas without apparent loss of energy and angular momentum: no electromagnetic emission from their surface is observed, see e.g. Refs. [53–55]. For a generic stationary and axisymmetric space-time, $E_{\rm ISCO}$ and $L_{\rm ISCO}$ can be computed numerically, as described in [33]. Here I assume that $\tilde{q}$ is a constant and does not change as the object increases its mass and is spun up, but this is not true in general. For example, in the case of neutron stars, $\tilde{q}$ depends on the mass of the body [47]. If the astrophysical BH candidates were objects with an anomalous quadrupole moment depending strongly on the mass of the body, objects with different mass could have a different equilibrium spin parameter.

Neglecting the effect of the radiation captured by the object and the presence of magnetic fields in the plunging region, in Fig. 7 I show $da_*/d\ln M$ as a function of the spin parameter a_* for some values of the anomalous quadrupole moment $\tilde{q}$. The value of the equilibrium spin parameter a_*^{eq} for these cases is reported in Tab. 1. In Fig. 7, the solid red curve is for a BH ($\tilde{q} = 0$) and has been computed by using Boyer–Lindquist coordinates. Indeed, even if the Kerr metric is included in the MMS solution, neither the form of the metric presented in [44, 45], nor the one discussed in Sec. 2 are suitable for numerical calculations, as they would require that the parameter b is an imaginary number. For a similar reason, for a given $\tilde{q} \neq 0$ we cannot study the evolution of the spin parameter from $a_* = 0$ to $a_* = a_*^{eq}$, but from some value $a_*^{in} > 0$, depending on $\tilde{q}$. When $da_*/d\ln M > 0$, the accretion process spins the compact body up. When $da_*/d\ln M < 0$, the compact body is spun down. The equilibrium spin parameter is thus the one for which $da_*/d\ln M = 0$. In Fig. 8, I show the quantity $da_*/d\ln M$ for a BH (green dotted curve) and for three compact objects with the same anomalous quadrupole moment $\tilde{q} = \pm 1.0$, but different higher order moments: the

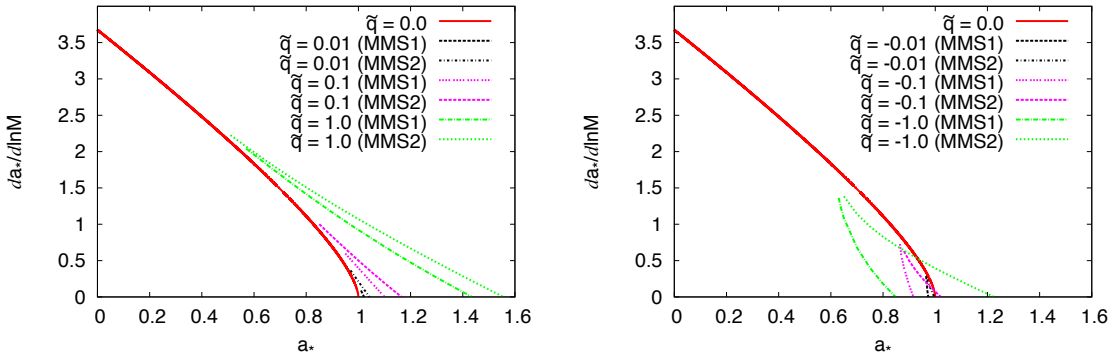

Figure 7. $da_*/d\ln M$ as a function of a_* for different value of the anomalous quadrupole moment $\tilde{q}$. The red solid curve is for the case of a BH ($\tilde{q} = 0$). Left panel: cases with $\tilde{q} \geq 0$. Right panel: cases with $\tilde{q} \leq 0$.

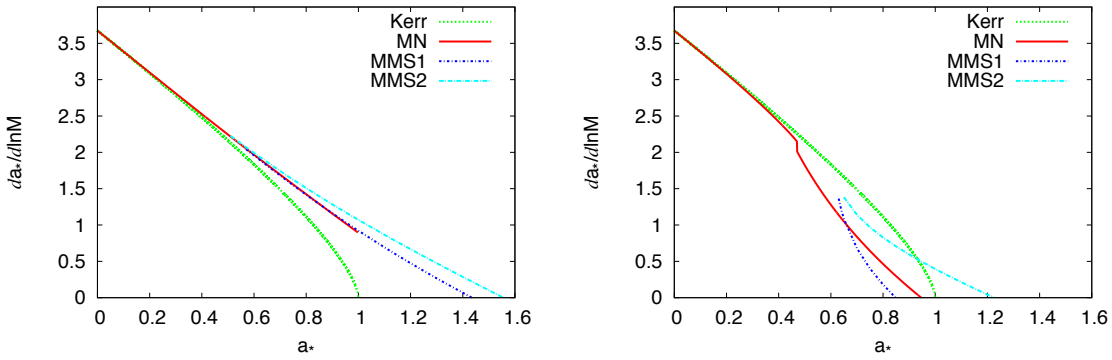

Figure 8. Comparison of the function $da_*/d\ln M$ for the case of the MN solution with the MMS1 and MMS2 solution with the same value of the anomalous quadrupole moment. Left panel: $\tilde{q} = 1$. Right panel: $\tilde{q} = -1$. The MN solution can be used till $a_* = 1$. The green dotted curve is for the case of a BH.

subclass of MN metrics discussed in Ref. [38] (red solid curve), MMS1 (dark-blue dotted-dashed curve), and MMS2 (light-blue dotted-dashed curve).

Fig. 9 shows the evolution of the spin parameter a_* as a function of M/M_0, the mass to initial mass ratio. Eq. (4.1) is numerically integrated from a_*^{in}, with M/M_0 equal to the one of the Kerr solution with the same spin parameter.

5 Discussion

As the values of $E_{\rm ISCO}$ and $L_{\rm ISCO}$ in Eq. (4.1) depend on the metric of the space-time, compact objects with different quadrupole (or higher) moment have a different equilibrium spin parameter a_*^{eq}. Figs. 7, 9, and Tab. 1 can be qualitatively understood in term of the inner radius of the disk r_{in}: for a given spin parameter, $da_*/d\ln M$ depends on $L_{\rm ISCO}/E_{\rm ISCO}$, which typically increases/decreases if r_{in} is larger/smaller. Fig. 10 shows the value of the inner radius of the disk in Schwarzschild coordinates (see Eq. (A.5) in App. A) as a function of the spin parameter. For instance, the MMS1 solutions with $\tilde{q} < 0$ have $a_*^{eq} < 1$; as we

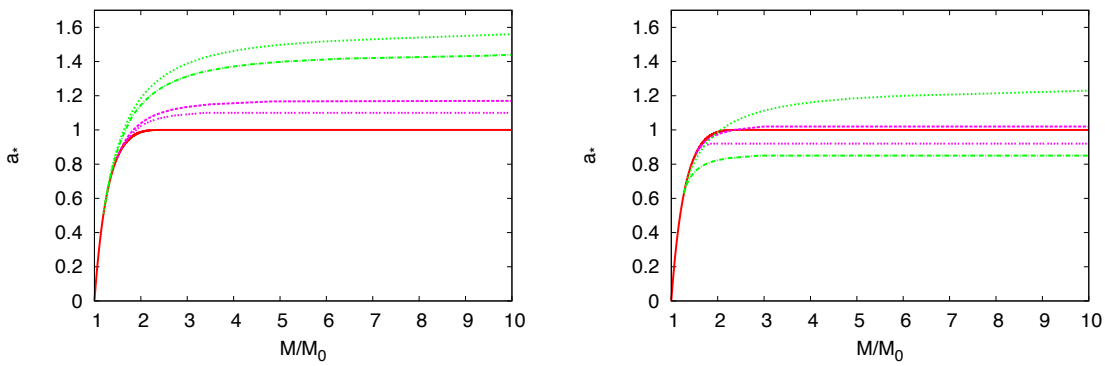

Figure 9. Evolution of the spin parameter a_* as a function of M/M_0. The color and the style of the curves for any $\tilde{q}$ is the same of Fig. 7 (the cases $\tilde{q} = \pm 0.001$ are not shown because for them the evolution of a_* can be studied only in a very limited interval of the spin parameter). The red solid curve is for the case of a BH ($\tilde{q} = 0$). Left panel: cases with $\tilde{q} \geq 0$. Right panel: cases with $\tilde{q} \leq 0$.

$\tilde{q}$	a_*^{eq} (MMS1)	a_*^{eq} (MMS2)	a_*^{eq} (Kerr)
1.0	1.44	1.56	–
0.1	1.10	1.17	–
0.01	1.02	1.04	–
0.0	–	–	1.00
-0.01	0.97	0.997	–
-0.1	0.92	1.02	–
-1.0	0.85	1.23	–

Table 1. Equilibrium spin parameter a_*^{eq} for the cases shown in Fig. 7.

can see, their inner disk's radius is smaller than the one in Kerr space-time for $|a_*| \leq a_*^{eq}$. The curves for the MMS1 solutions $\tilde{q} = -0.01$ and -0.1 in the right panel of Fig. 10 stop at $r_{in} = M$, which is equivalent to $x = 0$, because our coordinates cannot describe the space-time at smaller radii ($0 \leq x < +\infty$). These two cases have anyway to be taken with caution: there are regions with closed time-like curves with Schwarzschild radius larger than M, so even the surface of the compact object should be probably larger than M. Let us notice, however, that this happens for $a_* > a_*^{eq}$ and it can be neglected in the study of the evolution of the spin. As shown in Fig. 10, for sufficiently high values of the spin parameter, the inner radius of the disk always increases as a_* increases. This is not a surprise, because even in the Kerr space-time the radius of the ISCO reaches a minimum for $a_* \approx 1.089$, and then it increases as a_* increases [56].

The value of the inner radius of the disk depends inevitably on the choice of the coordinates; the comparison of this quantity for objects with different value of $\tilde{q}$ is thus not so meaningful. From this point of view, a more interesting quantity is the angular velocity of a gas particle at the inner radius of the disk, which is shown in Fig. 11. As we can see, the angular frequency at r_{in} can be very high around a very fast-rotating BH, while it is significantly lower for another compact object, regardless of its spin parameter. This can be

an interesting observational feature to test the Kerr nature of astrophysical BH candidates, because it implies that it is very difficult for an object that is not a BH to mimic a very fast-rotating BH. In other words, among the stationary and axisymmetric space-times, the Kerr solution is a very special case with peculiar properties and this is particularly true for $a_* \to 1$. Generally speaking, the accretion process onto an object with non-Kerr quadrupole moment looks more like the accretion onto a slow-rotating BH, but it can hardly present some features of a fast-rotating BH.

For fast-rotating objects, even deformations beyond the quadrupole moments are important for the properties of the space-time. In Fig. 12, I show the inner radius of the disk and the corresponding angular frequency of a gas particle around objects with $a_* = 0.99$ as a function of the anomalous quadrupole moment. The three curves represent three objects with same mass, spin, and quadrupole moment, but different higher order moments: the subclass of MN solutions discussed in [38], the MMS1 solution, and the MMS2 solution.

As already noticed in [38], Eq. (4.1) provides the correct evolution of the spin parameter if the compact object does not become unstable before reaching the equilibrium value a_*^{eq}. More in general, the accretion process can spin the body up, but there may exist other processes that spin it down. This is what should happen, for instance, in the case of a neutron star: the gas of the accretion disk can spin the neutron star up, but, when the rotational frequency of the object exceeds ~ 1 kHz, there are unstable modes that spin the neutron star down through the emission of gravitational waves [57]. If something similar happens for BH candidates, the maximum value of the spin parameter would be determined by the internal structure of these objects. The latter may spin down by emitting gravitational waves, presumably as a burst, potentially detectable by future experiments.

The fact that the accretion process can spin a compact object up to $a_* > 1$ can be relevant for the super-massive BH candidates at the center of galaxies, while it should be negligible for stellar-mass objects in X-ray binary systems. In general, the value of the spin parameter of a compact object is determined by the competition of three physical processes: the event creating the object, mergers, and gas accretion. For the stellar-mass BH candidates in X-ray binary systems, the value of their spin should reflect the one at the time of their creation. If they belong to low-mass X-ray binary systems, even swallowing the whole stellar companion they cannot change significantly their spin, because the mass of the stellar companion is much smaller. If they are in high-mass X-ray binary systems, even accreting at the Eddington limit they do not have enough time to grow before the explosion of the companion. On the contrary, for the super-massive objects in galactic nuclei the initial spin value is completely unimportant, as they have increased their mass by a few orders of magnitude from the original one. In the case of prolonged disk accretion, the object has the time to align itself with the disk and the process of gas accretion should dominate over mergers [36]. This picture is supported even by current estimates of the mean radiative efficiency of AGN [37]. As shown in [38], the alignment timescale is the same for BHs and objects with non-Kerr quadrupole moment, as long as $|\tilde{q}| \ll 100$.

6 Conclusions

The final product of the gravitational collapse of matter is thought to be a black hole and there are astrophysical evidences for the existence of dark objects that are too compact and too heavy to be relativistic stars or clusters of non-luminous bodies. In 4-dimensional general relativity, a black hole is completely specified by its mass M and by its spin parameter a_*,

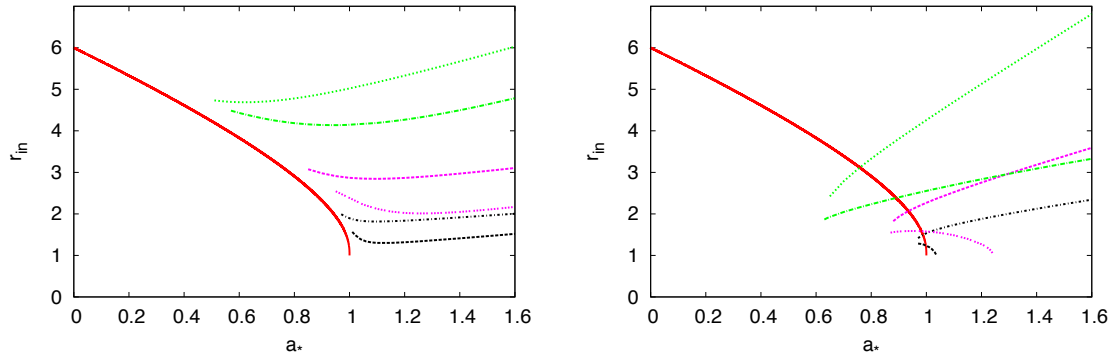

Figure 10. Inner radius of the accretion disk as a function of the spin parameter a_* for different values of the anomalous quadrupole moment $\tilde{q}$. The color and the style of the curves for any $\tilde{q}$ is the same of Fig. 7. Left panel: cases with $\tilde{q} \geq 0$. Right panel: cases with $\tilde{q} \leq 0$. Inner radius of the disk in Schwarzschild coordinates and in units of $M = 1$.

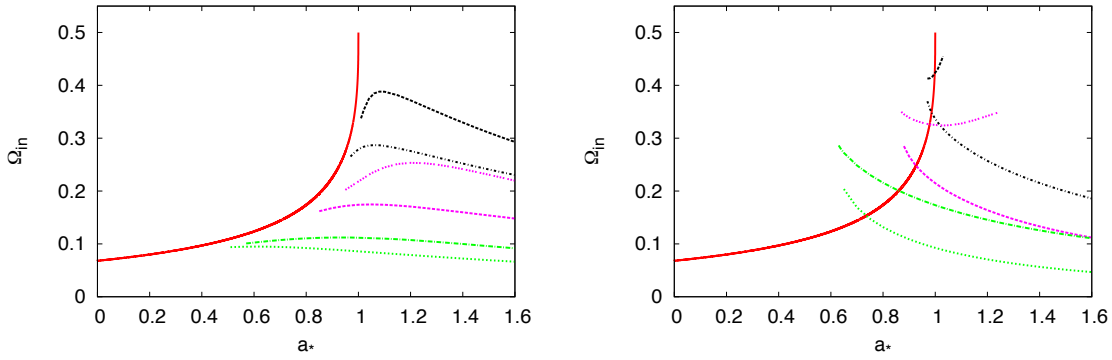

Figure 11. Angular velocity at the inner radius of the accretion disk as a function of the spin parameter a_* for different values of the anomalous quadrupole moment $\tilde{q}$. The color and the style of the curves for any $\tilde{q}$ is the same of Fig. 7. Left panel: cases with $\tilde{q} \geq 0$. Right panel: cases with $\tilde{q} \leq 0$. Ω_{in} is given in units of $M = 1$.

and it is subjected to the Kerr bound $|a_*| \leq 1$, which is the condition for the existence of the event horizon. The accretion process can spin a black hole up to $a_* \approx 0.998$ and at least some of the super-massive objects at the center of galaxies may be fast-rotating black holes with spin parameter close to this value.

The Kerr black hole paradigm is still based on a set of unproven assumptions. They sounded reasonable forty years ago, but they are more questionable today. There is no direct evidence that black hole candidates have an event horizon, while there are theoretical arguments suggesting new physics appearing at macroscopic scales [7–12]. If the astrophysical black hole candidates are not the objects predicted by general relativity, they are not subjected to the Kerr bound. Interestingly, the accretion process onto a body with non-Kerr quadrupole moment typically spins the object up to $a_* > 1$.

In Ref. [38], I used the Manko–Novikov solution to describe the exterior gravitational field of a generic compact body. I showed that in most cases the equilibrium spin parameter is larger than 1. However, the Manko–Novikov solution is valid only for $|a_*| < 1$ and therefore

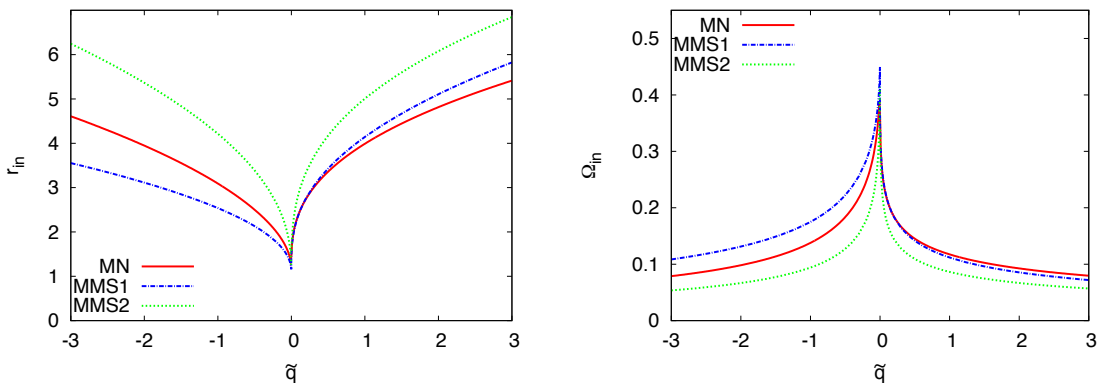

Figure 12. Left panel: inner radius of the disk for bodies with spin parameter $a_* = 0.99$ as a function of the anomalous quadrupole moment $\tilde{q}$ for the MN (red solid curve), MMS1 (blue dashed-dotted curve), and MMS2 (green dotted curve) solutions. Right panel: as in the left panel, for the angular velocity at the inner radius of the disk. Inner radius of the disk in Schwarzschild coordinates and in units of $M = 1$. Ω_{in} is given in units of $M = 1$.

it was impossible to study the accretion process for $a_* > 1$ and figure out the properties of the space-time around a super-spinning body. In the present paper, I considered the Manko–Mielke–Sanabria-Gómez solution, which can describe the gravitational field outside a compact body with non-Kerr quadrupole moment and spin parameter either smaller and larger than 1. I studied the basic properties of the space-times when $a_* > 1$, I discussed the evolution of the spin parameter, and I found its equilibrium value, see Figs. 7, 9, and Tab. 1. For fast-rotating objects, the accretion processes onto a black hole and onto a generic body are quite different. For example, only around a black hole can the inner radius of the disk be very small, while the angular frequency of the gas particles at the innermost circular orbit can be significantly higher than the one around another object.

The fact that the accretion process in a non-Kerr background can spin the compact body up to $a_* > 1$ is relevant for the research devoted to figure out how future observations can test the Kerr nature of the current astrophysical black hole candidates. The possibility that these objects can have spin parameter larger than 1 cannot be ignored and this is particularly true for experiments like LISA, whose detection relies on matched filtering.

Acknowledgments

I would like to thank Enrico Barausse, Shinji Mukohyama, and Naoki Yoshida for useful discussions. This work was supported by World Premier International Research Center Initiative (WPI Initiative), MEXT, Japan, and by the JSPS Grant-in-Aid for Young Scientists (B) No. 22740147.

A Coordinate systems

The canonical form of the line element of a generic stationary and axisymmetric space-time in quasi-cylindrical coordinates ρz is

$$ds^2 = -f\left(dt - \omega d\phi\right)^2 + \frac{e^{2\gamma}}{f}\left(d\rho^2 + dz^2\right) + \frac{\rho^2}{f}d\phi^2\,. \tag{A.1}$$

The relation between quasi-cylindrical coordinates ρz and prolate spheroidal coordinates xy is qiven by

$$\rho = k\sqrt{(x^2-1)(1-y^2)}\,, \quad z = kxy\,, \tag{A.2}$$

where k is a constant. The inverse relation is

$$x = \frac{R_+ + R_-}{2k}\,, \quad y = \frac{R_+ - R_-}{2k}\,, \tag{A.3}$$

where $R_\pm = \sqrt{\rho^2 + (z \pm k)^2}$. Through the formal transformation $x \to ix$ and $k \to -ik$, where i is the imaginary unit, one changes the prolate spheroidal coordinates into oblate spheroidal coordinates. The relation between the quasi-cylindrical coordinates and the oblate spheroidal coordinates is therefore given by

$$\rho = k\sqrt{(x^2+1)(1-y^2)}\,, \quad z = kxy\,. \tag{A.4}$$

Lastly, the relation between quasi-cylindrical coordinates and Schwarzschild coordinates is [58]

$$\rho = \sqrt{r^2 - 2Mr + a^2}\,\sin\theta\,, \quad z = (M-r)\cos\theta\,, \tag{A.5}$$

where M is the mass and $a = J/M$ the specific spin angular momentum.

Prolate spheroidal coordinates are suitable for describing the space-time around slow-rotating objects, while oblate spheroidal coordinates are suitable in the case of fast-rotating objects. In the special case of the Kerr space-time, prolate spheroidal coordinates can be used only for BHs, oblate spheroidal coordinates only for Kerr naked singularity (see App. B). The left (right) panel of Fig. 13 shows some curves with constant prolate (oblate) coordinate x on the ρz-plane for $k = 1.5\,M$. Fig. 14 shows instead some curves with constant Schwarzschild radial coordinate, still on the ρz-plane, for $a = 0.8\,M$ (left panel) and $a = 1.2\,M$ (right panel). In the former case, the quasi-cylindrical coordinates cover the space with Schwarzschild radial coordinate $r \geq r_H = M + \sqrt{M^2 - a^2}$ and the surface with radial coordinate $r = r_H$ corresponds to the segment $\rho = 0$ and $|z| < \sqrt{M^2 - a^2}$. Here r_H is equal to the Schwarzschild radial coordinate of the even horizon of a Kerr BH with spin a. When $|a| > M$, the quasi-cylindrical coordinates can be used to describe the region $r > M$ (otherwise there is not a one-to-one correspondence between the two coordinate systems) and the circle with radius $r = M$ reduces to the segment $|\rho| < \sqrt{a^2 - M^2}$ and $z = 0$ on the ρz-plane. For non-Kerr objects, prolate (oblate) spheroidal coordinates are still adequate only for slow-rotating (fast-rotating) objects, but in general the value of the spin a separating the two cases is not M any more.

B Kerr space-time in spheroidal coordinates

In prolate spheroidal coordinates, the line element (A.1) is

$$\begin{aligned} ds^2 = &-f\left(dt - \omega d\phi\right)^2 + \frac{k^2 e^{2\gamma}}{f}\left(x^2 - y^2\right)\left(\frac{dx^2}{x^2-1} + \frac{dy^2}{1-y^2}\right) + \\ &+ \frac{k^2}{f}\left(x^2-1\right)\left(1-y^2\right)d\phi^2\,. \end{aligned} \tag{B.1}$$

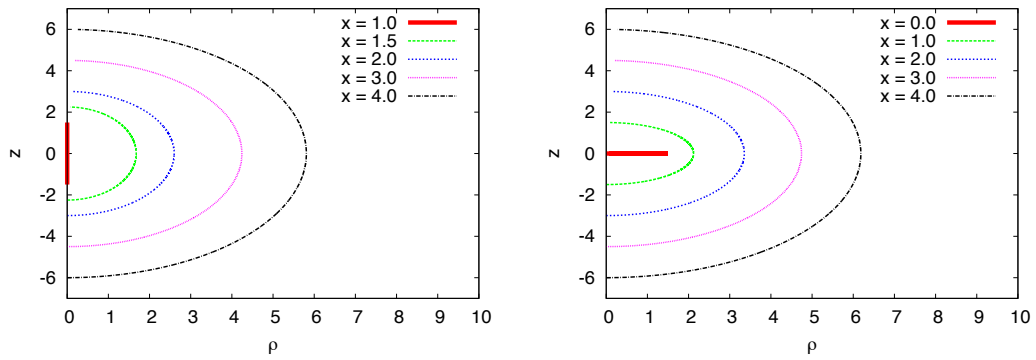

Figure 13. Curves with constant prolate spheroidal coordinate x (left panel) and oblate spheroidal coordinate x (right panel) on the ρz-plane. ρ and z are given in units of $M = 1$. $k = 1.5\,M$.

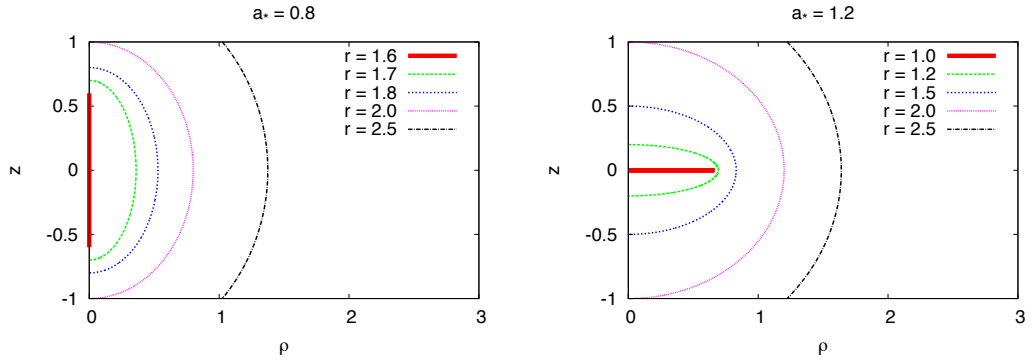

Figure 14. Curves with constant Schwarzschild radial coordinate on the ρz-plane, for $a_* = 0.8$ (left panel) and $a_* = 1.2$ (right panel). ρ and z are given in units of $M = 1$.

In the Kerr space-time

$$f = \frac{A}{B}\,, \quad \omega = -(1-y^2)\frac{C}{A}\,, \quad e^{2\gamma} = \frac{A}{k^2(x^2-y^2)}\,, \tag{B.2}$$

where A, B, and C are given by

$$A = k^2(x^2-1) - a^2(1-y^2)\,, \quad B = (kx+M)^2 + a^2y^2\,, \quad C = 2aM(kx+M)\,. \tag{B.3}$$

Here M is the mass, $a = J/M$ is the specific spin angular momentum, and $k = \sqrt{M^2 - a^2}$. Prolate spheroidal coordinates can be used to describe only BHs ($|a_*| < 1$) and the surface $x = 1$ is the BH event horizon. The transformation $x \to ix$ and $k \to -ik$ changes the prolate spheroidal coordinates into oblate spheroidal coordinates, which can be used to describe the space region around a Kerr naked singularity ($|a_*| > 1$) with Schwarzschild radial coordinate $r > M$. Fig. 15 shows the infinite redshift surface $g_{tt} = 0$ (red solid curve) and the event horizon (blue dotted curve) of a BH with $a_* = 0.8$ in *prolate* spheroidal coordinates xy (left panel), quasi-cylindrical coordinates ρz (central pane), and Schwarzschild coordinates $r\theta$ (right panel). Fig. 16 shows the infinite redshift surface of a Kerr naked singularity with $a_* = 1.2$ in *oblate* spheroidal coordinates xy (left panel), quasi-cylindrical coordinates ρz (central pane), and Schwarzschild coordinates $r\theta$ (right panel).

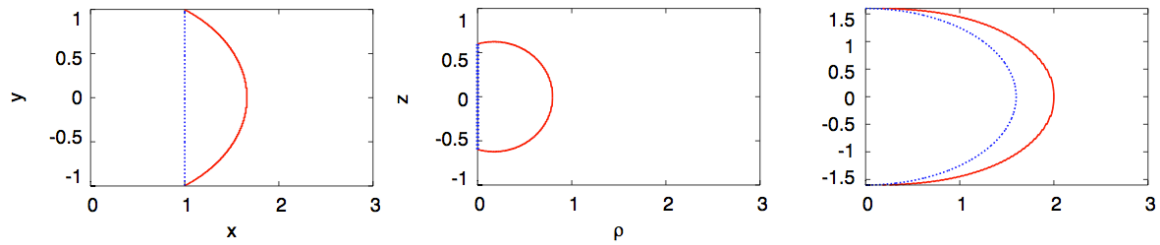

Figure 15. Infinite redshift surface $g_{tt} = 0$ (red solid curves) and event horizon (blue dotted curves) in Kerr space-time with $a_* = 0.8$ in prolate spheroidal coordinates xy (left panel), quasi-cylindrical coordinates ρz (central panel), and Schwarzschild coordinates $r\theta$ (right panel). ρ, z, and r are given in units of $M = 1$.

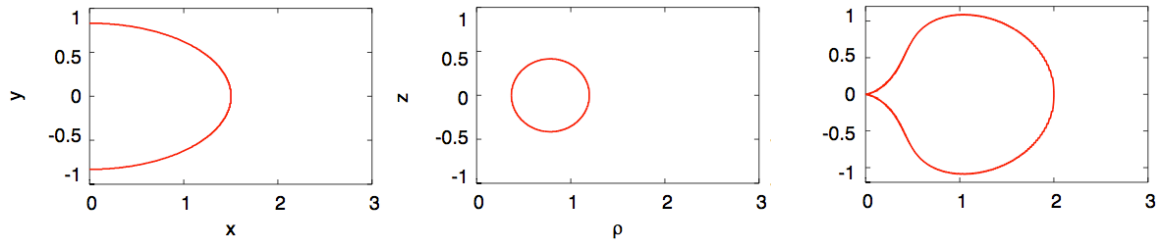

Figure 16. Infinite redshift surface $g_{tt} = 0$ in Kerr space-time with $a_* = 1.2$ in oblate spheroidal coordinates xy (left panel), quasi-cylindrical coordinates ρz (central panel), and Schwarzschild coordinates $r\theta$ (right panel). ρ, z, and r are given in units of $M = 1$.

References

[1] A. P. Cowley, Ann. Rev. Astron. Astrophys. **30**, 287 (1992).

[2] J. Kormendy and D. Richstone, Ann. Rev. Astron. Astrophys. **33**, 581 (1995).

[3] C. E. . Rhoades and R. Ruffini, Phys. Rev. Lett. **32**, 324 (1974).

[4] V. Kalogera and G. Baym, Astrophys. J. **470**, L61 (1996).

[5] E. Maoz, Astrophys. J. **494**, L181 (1998).

[6] M. A. Abramowicz, W. Kluzniak and J. P. Lasota, Astron. Astrophys. **396**, L31 (2002) [arXiv:astro-ph/0207270].

[7] S. V. Babak, L. P. Grishchuk, Int. J. Mod. Phys. **D12**, 1905-1960 (2003). [gr-qc/0209006].

[8] J. L. Karczmarek, J. M. Maldacena, A. Strominger, JHEP **0601**, 039 (2006). [hep-th/0411174].

[9] E. G. Gimon, P. Horava, Phys. Lett. **B672**, 299-302 (2009). [arXiv:0706.2873 [hep-th]].

[10] L. Modesto, Int. J. Theor. Phys. **49**, 1649-1683 (2010). [arXiv:0811.2196 [gr-qc]].

[11] S. D. Mathur, Class. Quant. Grav. **26**, 224001 (2009). [arXiv:0909.1038 [hep-th]].

[12] D. Marolf, Gen. Rel. Grav. **42**, 2337-2343 (2010). [arXiv:1005.2999 [gr-qc]].

[13] B. Carter, Phys. Rev. Lett. **26**, 331 (1971).

[14] D. C. Robinson, Phys. Rev. Lett. **34**, 905 (1975).

[15] P. T. Chrusciel and J. Lopes Costa, arXiv:0806.0016 [gr-qc].

[16] R. Geroch, J. Math. Phys. **11**, 2580 (1970).

[17] R. Hansen, J. Math. Phys. **15**, 46 (1974).

[18] F. D. Ryan, Phys. Rev. D **52**, 5707 (1995).

[19] F. D. Ryan, Phys. Rev. D **56**, 1845 (1997).

[20] C. Bambi, arXiv:1102.0616 [gr-qc].

[21] N. A. Collins and S. A. Hughes, Phys. Rev. D **69**, 124022 (2004) [arXiv:gr-qc/0402063].

[22] K. Glampedakis and S. Babak, Class. Quant. Grav. **23**, 4167 (2006) [arXiv:gr-qc/0510057].

[23] L. Barack and C. Cutler, Phys. Rev. D **75**, 042003 (2007) [arXiv:gr-qc/0612029].

[24] J. R. Gair, C. Li and I. Mandel, Phys. Rev. D **77**, 024035 (2008) [arXiv:0708.0628 [gr-qc]].

[25] T. A. Apostolatos, G. Lukes-Gerakopoulos and G. Contopoulos, Phys. Rev. Lett. **103**, 111101 (2009) [arXiv:0906.0093 [gr-qc]].

[26] S. J. Vigeland and S. A. Hughes, Phys. Rev. D **81**, 024030 (2010) [arXiv:0911.1756 [gr-qc]].

[27] G. Lukes-Gerakopoulos, T. A. Apostolatos and G. Contopoulos, Phys. Rev. D **81**, 124005 (2010) [arXiv:1003.3120 [gr-qc]].

[28] C. Bambi and K. Freese, Phys. Rev. D **79**, 043002 (2009) [arXiv:0812.1328 [astro-ph]].

[29] C. Bambi and N. Yoshida, Class. Quant. Grav. **27**, 205006 (2010) [arXiv:1004.3149 [gr-qc]].

[30] T. Johannsen and D. Psaltis, Astrophys. J. **718**, 446 (2010) [arXiv:1005.1931 [astro-ph.HE]]

[31] N. Wex and S. Kopeikin, Astrophys. J. **514**, 388 (1999) [arXiv:astro-ph/9811052].

[32] D. Psaltis and T. Johannsen, arXiv:1011.4078 [astro-ph.HE].

[33] C. Bambi and E. Barausse, arXiv:1012.2007 [gr-qc].

[34] K. S. Thorne, Astrophys. J. **191**, 507 (1974).

[35] M. Volonteri, P. Madau, E. Quataert and M. J. Rees, Astrophys. J. **620**, 69 (2005) [arXiv:astro-ph/0410342].

[36] E. Berti and M. Volonteri, Astrophys. J. **684**, 822 (2008) [arXiv:0802.0025 [astro-ph]].

[37] J. -M. Wang, Y. -M. Chen, L. C. Ho *et al.*, Astrophys. J. **642**, L111-L114 (2006). [astro-ph/0603813].

[38] C. Bambi, arXiv:1101.1364 [gr-qc].

[39] C. Bambi, K. Freese, T. Harada, R. Takahashi and N. Yoshida, Phys. Rev. D **80**, 104023 (2009) [arXiv:0910.1634 [gr-qc]].

[40] C. Bambi, T. Harada, R. Takahashi and N. Yoshida, Phys. Rev. D **81**, 104004 (2010) [arXiv:1003.4821 [gr-qc]].

[41] C. Bambi and N. Yoshida, Phys. Rev. D **82**, 064002 (2010) [arXiv:1006.4296 [gr-qc]].

[42] C. Bambi and N. Yoshida, Phys. Rev. D **82**, 124037 (2010) [arXiv:1009.5080 [gr-qc]].

[43] V. S. Manko and I. D. Novikov, Class. Quant. Grav. **9**, 2477 (1992).

[44] V. S. Manko, E. W. Mielke and J. D. Sanabria-Gomez, Phys. Rev. D **61**, 081501 (2000) [arXiv:gr-qc/0001081].

[45] V. S. Manko, J. D. Sanabria-Gomez and O. V. Manko, Phys. Rev. D **62**, 044048 (2000).

[46] M. Calvani, R. Catenacci and F. Salmistraro, Lett. Nuovo Cim. **16**, 460 (1976).

[47] W. G. Laarakkers and E. Poisson, Astrophys. J. **512**, 282 (1999).

[48] H. Kodama and W. Hikida, Class. Quant. Grav. **20**, 5121 (2003).

[49] B. Carter, Commun. Math. Phys. **10**, 280 (1968).

[50] J. M. Bardeen, Nature **226**, 64 (1970).

[51] C. F. Gammie, S. L. Shapiro and J. C. McKinney, Astrophys. J. **602**, 312 (2004).

[52] S. L. Shapiro, Astrophys. J. **620**, 59 (2005).

[53] M. R. Garcia, J. E. McClintock, R. Narayan, P. Callanan and S. S. Murray, Astrophys. J. **553**, L47 (2001) [arXiv:astro-ph/0012452].

[54] R. Narayan, J. S. Heyl, Astrophys. J. **574**, L139-L142 (2002). [astro-ph/0203089].

[55] A. E. Broderick, A. Loeb and R. Narayan, Astrophys. J. **701**, 1357 (2009) [arXiv:0903.1105 [astro-ph.HE]].

[56] R. Takahashi, T. Harada, Class. Quant. Grav. **27**, 075003 (2010). [arXiv:1002.0421 [astro-ph.HE]].

[57] N. Andersson, D. I. Jones, K. D. Kokkotas and N. Stergioulas, Astrophys. J. **534**, L75 (2000).

[58] E. N. Glass, Phys. Rev. **D7**, 3127-3130 (1973).